Carcinogenesis vol.35 no.9 pp.2142–2153, 2014
doi:10.1093/carcin/bgu143
Advance Access publication July 1, 2014

Androgen deprivation induces phenotypic plasticity and promotes resistance to molecular targeted therapy in a *PTEN*-deficient mouse model of prostate cancer

Marco A.De Velasco[1,2,*], Motoyoshi Tanaka[3], Yutaka Yamamoto[1], Yuji Hatanaka[1], Hiroyuki Koike[1], Kazuto Nishio[2], Kazuhiro Yoshikawa[4] and Hirotsugu Uemura[1]

[1]Department of Urology and [2]Department of Genome Biology, Kinki University Faculty of Medicine, Osaka-Sayama, Osaka 589-8511, Japan, [3]Department of Urology, Iga City General Hospital, Iga, Mie 518-0823, Japan and [4]Promoting Center for Clinical Research, Aichi Medical University School of Medicine, Nagakute, Aichi 480-1195, Japan

*To whom correspondence should be addressed. Tel: +81-72-366-0221 ext. 3523; Fax: +81-72-365-6273;
Email: mdev@med.kindai.ac.jp

Castration-resistant prostate cancer is an incurable heterogeneous disease that is characterized by a complex multistep process involving different cellular and biochemical changes brought on by genetic and epigenetic alterations. These changes lead to the activation or overexpression of key survival pathways that also serve as potential therapeutic targets. Despite promising preclinical results, molecular targeted therapies aimed at such signaling pathways have so far been dismal. In the present study, we used a *PTEN*-deficient mouse model of prostate cancer to show that plasticity in castration-resistant tumors promotes therapeutic escape. Unlike castration-naïve tumors which depend on androgen receptor and PI3K/AKT signal activation for growth and survival, castration-resistant tumors undergo phenotypic plasticity leading to increased intratumoral heterogeneity. These tumors attain highly heterogeneous phenotypes that are characterized by cancer cells relying on alternate signal transduction pathways for growth and survival, such as mitogen-activated protein kinase and janus kinase/signal transducer and activator of transcription, and losing their dependence on PI3K signaling. These features thus enabled castration-resistant tumors to become insensitive to the therapeutic effects of PI3K/AKT targeted therapy. Overall, our findings provide evidence that androgen deprivation drives phenotypic plasticity in prostate cancer cells and implicate it as a crucial contributor to therapeutic resistance in castration-resistant prostate cancer. Therefore, incorporating intratumoral heterogeneity in a dynamic tumor model as a part of preclinical efficacy determination could improve prediction for response and provide better rationale for the development of more effective therapies.

Introduction

Castration-resistant prostate cancer (CRPC) is an incurable disease that is causally related to continued transactivation of the androgen receptor (AR) despite the low androgen levels resulting from physical or chemical castration. AR is an important mediator of prostate cancer progression and considerable evidence exists to suggest that CRPC continues to depend on the AR signaling axis for continued cellular growth and survival (1). Activation of AR-regulated genes in CRPC indicates AR transcriptional activation, perhaps resulting from any number of alterations such as AR amplification/overexpression, AR mutations, intracrine AR production, sensitization to low levels of AR, by the overexpression of AR cofactors, constitutively active messenger RNA splice variants of AR, and crosstalk with pro-survival pathways (2,3). Furthermore, the deregulation of signal transduction pathways, resulting from oncogenic mutations, can lead to androgen independent proliferation of cancer cells therefore augmenting resistance to AR-targeted therapies (4,5).

The deregulation of signal transduction pathways that promote tumor growth and progression can occur through various known mechanisms such as the loss of tumor suppressor function, gain of function due to oncogenic mutations, gene amplification and upregulation of upstream signal receptors (6). A greater understanding of the signal transduction network and its role in disease function has led to the identification of key networks and relevant signaling molecules that represent attractive drug targets for cancer therapy. Unfortunately, most targeting agents have failed to meet expectations in the clinical setting due to poor efficacy, which is attributed due to poor predictability from unreliable traditional preclinical models (7). Traditional *in vivo* efficacy models using grafted tumors derived from clonal human cancer cell lines show a lack of intratumor heterogeneity, a feature common in autochthonous tumors. Tumor heterogeneity provides a high degree of redundancy and contributes to acquired tumor "robustness," that is, the ability to maintain stable functioning despite various perturbations (8). Cancer cells will exploit this characteristic in their natural evolution to ensure survival and overcome treatment therapies (9). Recently, the whole concept of preclinical to clinical modeling for cancer therapy has changed with the development of genetically engineered mice. These mice are designed to develop tumors *in situ* that originate from normal cells and replicate mutational changes seen in human cancers, thus providing a more clinically relevant model.

Our goal was to utilize a faithful mouse model of prostate cancer to characterize the dynamic evolution of CRPC resistance and survival. To do so, we generated a genetically engineered mouse model of prostate cancer based on the conditional inactivation of the tumor suppressor phosphatase and tensin homolog (*PTEN*). *PTEN* is broadly expressed during development and adulthood and encodes a lipid phosphatase that functions as an inhibitor of the PI3K/AKT pathway (10). *PTEN* function loss as a result of mutations, deletions, or promoter methylation silencing, occurs at a high frequency in human prostate cancer and correlates with increased AKT-1 phosphorylation; and is consequently associated with a poor prognosis and initiates downstream targets that modulate a wide range of cellular processes associated with the progression of tumor cell growth and survival (11–13). Although other *PTEN*-deficient mouse models have been established and characterized, there is still a wide degree of variation with regards to tumor latency, progression and survival (14). Factors that have probably contributed to such variations include differences in the promoter used to drive *PTEN* inactivation and mixed genetic backgrounds. Therefore, a conditional knockout mouse model of prostate cancer, driven by a prostate-specific promoter, on a pure background strain would be desired in order to characterize intratumoral heterogeneity during the natural progression and transformation to CRPC.

Materials and methods

Reagents and antibodies

Everolimus and U0126 were purchased from L.C. Labs. Antibodies used in this study are listed in Supplementary Table 1, available at *Carcinogenesis* Online.

Generation of transgenic mice

PSA^{Cre} mice were kindly provided by Dr. Milbrandt (University of Alabama at Birmingham School of Medicine) (15) and $PTEN^{loxP/loxP}$ mice were kindly provided by Dr. Mak (Amgen Institute Ontario Cancer Institute and University of Toronto) (16). PSA^{Cre} mice use the well characterized *PSA* promoter fragment that only targets expression to the prostate epithelial cells (17). $PTEN^{loxP/loxP}$

Abbreviations: ADT, androgen deprivation therapy; AR, androgen receptor; CRPC, castration-resistant prostate cancer; p-ERK, extracellular signal-regulated kinase; GUT, genitourinary tract; JAK/STAT, janus kinase/signal transducer and activator of transcription; MAPK, mitogen-activated protein kinase; mTOR, mammalian target of rapamycin; PI3K, phosphoinositide 3-kinase; PTEN, phosphatase and tensin homolog.

mice contain the conditional targeting vector that was constructed to delete exons 4 and 5 of the *PTEN* gene by homologous recombination (16). To generate $PSA^{Cre};PTEN^{loxP/loxP}$ mice, we crossed PSA^{Cre} mice with $PTEN^{loxP/loxP}$ mice to produce $PSA^{Cre};PTEN^{lox/+}$ mice. $PSA^{Cre};PTEN^{lox/+}$ were then backcrossed to produce $PSA^{Cre};PTEN^{loxP/loxP}$ mice. $PSA^{Cre};PTEN^{loxP/loxP}$ founders were then used to expand and establish a $PSA^{Cre};PTEN^{loxP/loxP}$ colony of mice expressing a homozygous deletion of *PTEN*. All mice were from the C57BL/6 strain background. For androgen ablation, mice were anesthetized and surgically castrated. This study was approved by the Institutional Review Committee at Kinki University Faculty of Medicine. Mice were housed in accordance with institutional guidelines and procedures were carried out in compliance with the standards for use of laboratory animals.

PCR genotyping

Genotyping for the *Cre* recombinase and *PTEN* genes was performed by PCR using tail biopsy DNA. DNA was extracted using the alkaline extraction method. Briefly, tail biopsies were incubated in 50 mM NaOH at 95°C for 10 m and neutralized with Tris–HCl (pH 8.0). PCR primers used for genotyping are as follows: *PSA-Cre*, sense-GC CTA TATC CCAAAGGAACAGAAG, antisense-CCTTCCTCTAGGTCCTTTAGGAGG; *PTEN*, sense-C TCCTCT ACTCCATTCTTCCC, antisense-ACTC CCACCA ATGAA CAAAC. PCR reaction conditions were as follows: initial denaturation at 94°C for 1 min, 35-cycle amplification at 94 C for 25 s, 60 C for 30 s and 72 C for 45 s, followed by final extension at 72 C for 10 additional minutes.

Histology and immunohistochemistry

Mice were killed and the whole genitourinary tract (GUT) was excised *en bloc*, weighed and fixed overnight in 10% neutral buffered formalin. For the collection of protein, half of the prostate was dissected and stored at 80 C. Samples were then processed for histology. For immunohistochemical analysis (IHC), additional slides were sectioned and stained with an ABC kit following standard protocols described previously (18). Histopathological classification of prostate lesions was performed according to the criteria proposed by the Bar Harbor Classification system (19,20). Assessment of staining was performed with ImageJ analysis software (http://imagej.nih.gov/ij/).

Terminal deoxynucleotidyl transferase-mediated dUTP nick end labeling assay

Terminal deoxynucleotidyl transferase-mediated dUTP nick end labeling assays were determined with the *In Situ* Cell Death Detection Kit (Roche) according to methods described previously (18).

Western blot analysis

Protein extraction was performed using a protease inhibitor cocktail (Sigma). Standard immunoblotting methods were carried out as described previously (18). Semi-quantitative densitometric analyses were performed with ImageJ analysis software. For all densitometric analyses, protein levels were normalized to glyceraldehyde 3-phosphate dehydrogenase or total protein.

Drug intervention studies

Drug efficacy studies were performed on 16-week-old homozygous *PTEN*-mutant mice harboring castration-naïve and CRPC. Mice were randomized and assigned to treatment groups consisting of everolimus (gavage, 10 mg/kg, 3×/week) or U0126 (i.p. 20 mg/kg/d) for 4 weeks. Everolimus was formulated 2% (w/v) in dimethyl sulfoxide and diluted with sterile dH_2O. U0126 was formulated 50 µmol/l in dimethyl sulfoxide and diluted with saline. Mice were killed and the GUTs were removed, weighed, imaged and processed for histopathological, IHC and WB analysis.

Tumor burden and efficacy determination

Tumor burden was determined by the weight of the GUT. Tumor growth rates were calculated based on the following exponential growth formula: $P(t) = P_0e^{rt}$, where $P(t)$ = time, P_0 = initial time, r = growth rate and t = time period. Antitumor efficacy was determined by differences in GUT weight or prostate surface area.

Survival studies

The eligibility criteria for mice included in the survival studies were palpable tumors >1 cm in diameter, healthy appearance and no previous body weight loss. Study endpoints were overall survival, disease progression and tumor burden. Disease progression was defined as expiry, tumor growth >2 cm in diameter, >25% body weight loss from baseline, >10% body weight loss in one week or poor general condition as determined by the technical staff.

Statistical analysis

Data were statistically analyzed using the Student's *t*-test for paired analysis, one-way analysis of variance for multiple comparisons and polynomial regression analysis for tumor growth dynamics. Kaplan–Meier survival curves using the log-rank test were used to measure survival. Differences were considered to be significant at $P < 0.05$. Statistical analysis was carried out using SigmaStat 3.5 (Systat Software.)

Results

Generation of prostate-specific PTEN-knockout mice

To establish a rational murine model of prostate cancer, we generated $PSA^{Cre};PTEN^{loxP/loxP}$ transgenic mice by cross breeding PSA^{Cre} and $PTEN^{loxP/loxP}$ and backcrossing the heterozygous progeny to create prostate-specific heterozygous- and homozygous-*PTEN* mutant progeny. We ensured effective recombination and transmission of deleted *PTEN* and *Cre* through the germ line by the PCR method using genomic DNA (Supplementary Figure 1A, available at *Carcinogenesis* Online). We established temporal and tissue-specific *Cre*-mediated recombination of DNA by analyzing the IHC expression Cre recombinase in the GUTs of homozygous *PTEN*-mutant mice at various time points of development. Cre recombinase-positive cells were observed in the dorsal lobe of the prostate as early as 6 weeks, the lateral lobe at 8 weeks and ventral lobe at 10 weeks (Supplementary Figure 1B, available at *Carcinogenesis* Online). A preliminary examination revealed the early formation of tumors (<20 weeks of age) in homozygous *PTEN*-mutant mice. Therefore, to confirm *Cre*-mediated inactivation of *PTEN* in mouse prostates, we examined the protein expression of PTEN and AKT. As expected, PTEN levels were considerably reduced in cancer cells of prostates from *PTEN*-deficient mice (Supplementary Figure 1C, available at *Carcinogenesis* Online). Accordingly phosphorylated AKT expression was upregulated in the absence of functional PTEN.

Tumor development in prostate-specific PTEN-knockout mice

To determine the ramifications of conditional *PTEN* allele inactivation in the prostate, we examined the GUTs from $PSA^{Cre};PTEN^{loxP/+}$ and $PSA^{Cre};PTEN^{loxP/loxP}$ mice at various time points. A histological assessment of prostate cancer development in heterozygous and homozygous *PTEN*-mutant mice is summarized in Supplementary Table 2, available at *Carcinogenesis* Online. Homozygous *PTEN*-mutant mice demonstrated gradually developed prostatic intraepithelial neoplasia as early as 8 weeks in the dorsolateral lobes that progressed to well-differentiated tumors (Figure 1A). By 15 weeks, virtually all mice had developed well-differentiated tumors in the dorsal and lateral lobes. From 20 weeks onward, all mice eventually developed adenocarcinomas in the lateral, dorsal and ventral prostate lobes; furthermore, tumors in the anterior prostate were infrequent.

Temporal assessment of tumor progression in homozygous PTEN-knockout mice

To better characterize the effects of *PTEN* inactivation as a key regulator driving cancer growth, we assessed tumor kinetics in homozygous *PTEN*-mutant mice over time. As the mice aged, obvious differences in tumor growth were clearly visible (Supplementary Figure 2A, available at *Carcinogenesis* Online). We used GUT weight as an indirect indicator for tumor burden in order to preserve normal tissue architecture. For the most part, complete inactivation of *PTEN* resulted in cubic tumor growth (Supplementary Figure 2B, available at *Carcinogenesis* Online). Significant tumor growth rates were observed from 10–25, 40–60, 60–70 and 70–90 weeks of age (5.7, 1.3, 2.94 and 4.15%, respectively, Figure 1B). At 50–60 weeks of age, 10% of mice developed distant spread of tumor metastases primarily in the loco-regional lymph nodes and occasionally in lung and liver (Supplementary Table 2, available at *Carcinogenesis* Online). By 75–90 weeks of age, the percentage of mice developing distant spread of disease increased to ~60%. Mean survival time for homozygous *PTEN*-mutant mice was 90.5 weeks [95% confidence interval (CI) 83.2–97.9, Figure 1C].

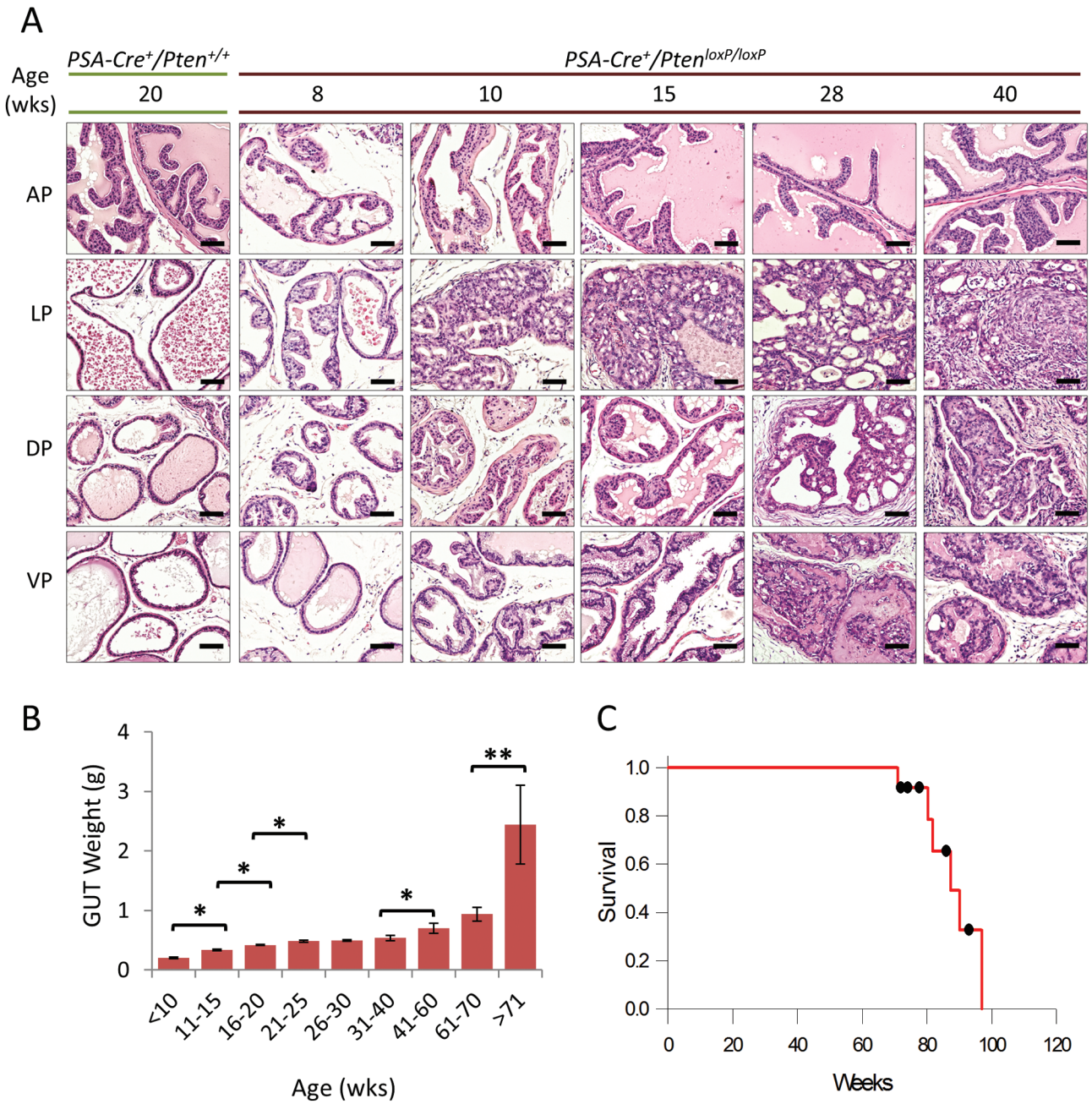

Fig. 1. Prostate cancer development in homozygous *PTEN*-mutant mice. (**A**) H&E stained tissue sections demonstrate the development and progression of cancer in the various lobes of the mouse prostate. As a reference, the first column shows the histology of a mouse with wild-type *PTEN*. Scale bars represent 100 µm. (**B**) Plot of temporal tumor growth expressed as the mean ± SE GUT weight (*$P < 0.01$, **$P < 0.05$). A scatter plot of (B) is shown in Supplementary Figure 3B, available at *Carcinogenesis* Online. (**C**) Kaplan–Meier curve showing cumulative survival rates ($n = 12$).

Androgen withdrawal responses in mouse PTEN-deficient prostate cancer

Prostate tumors are generally considered to be dependent on AR for growth and survival. However, recent data suggests that loss of *PTEN* promotes prostate cancer independently of the AR (4,5). To determine the consequences of *PTEN* inactivation and androgen withdrawal in this model, we examined the effects of surgical castration on established tumors. Homozygous *PTEN*-mutant mice initially responded to androgen withdrawal which was characterized by the marked atrophy and loss of nuclear AR expression (Figure 2A and B). However, as early as 8 weeks post-castration, nuclear translocation of AR is observed in some tumor cells, whereas by 12 weeks, numerous nests of tumor cells show restored nuclear AR.

The *PSA-Cre* promoter is dependent on AR for transgene expression, yet tumors continued to survive despite the withdrawal of androgens. Therefore, we examined the effects of castration on cre recombinase and PTEN expression, and PI3K pathway activation in age-matched castration-naïve and surgically-castrated 20-week-old homozygous *PTEN*-mutant mice at 4 or 10 weeks after castration. In this scenario, tumors from mice at 4 weeks post-castration represent androgen-sensitive tumors whereas those from mice 10 weeks post-castration represent CRPC. Overall, cre recombinase was expressed in all mice, even after castration (Figure 2C and Supplementary Figures 3A, available at *Carcinogenesis* Online). Overall expression of PTEN remained low in all groups, however, densitometric analysis revealed a trend of increased PTEN expression after castration (Supplementary Figure 3A, available at *Carcinogenesis* Online).

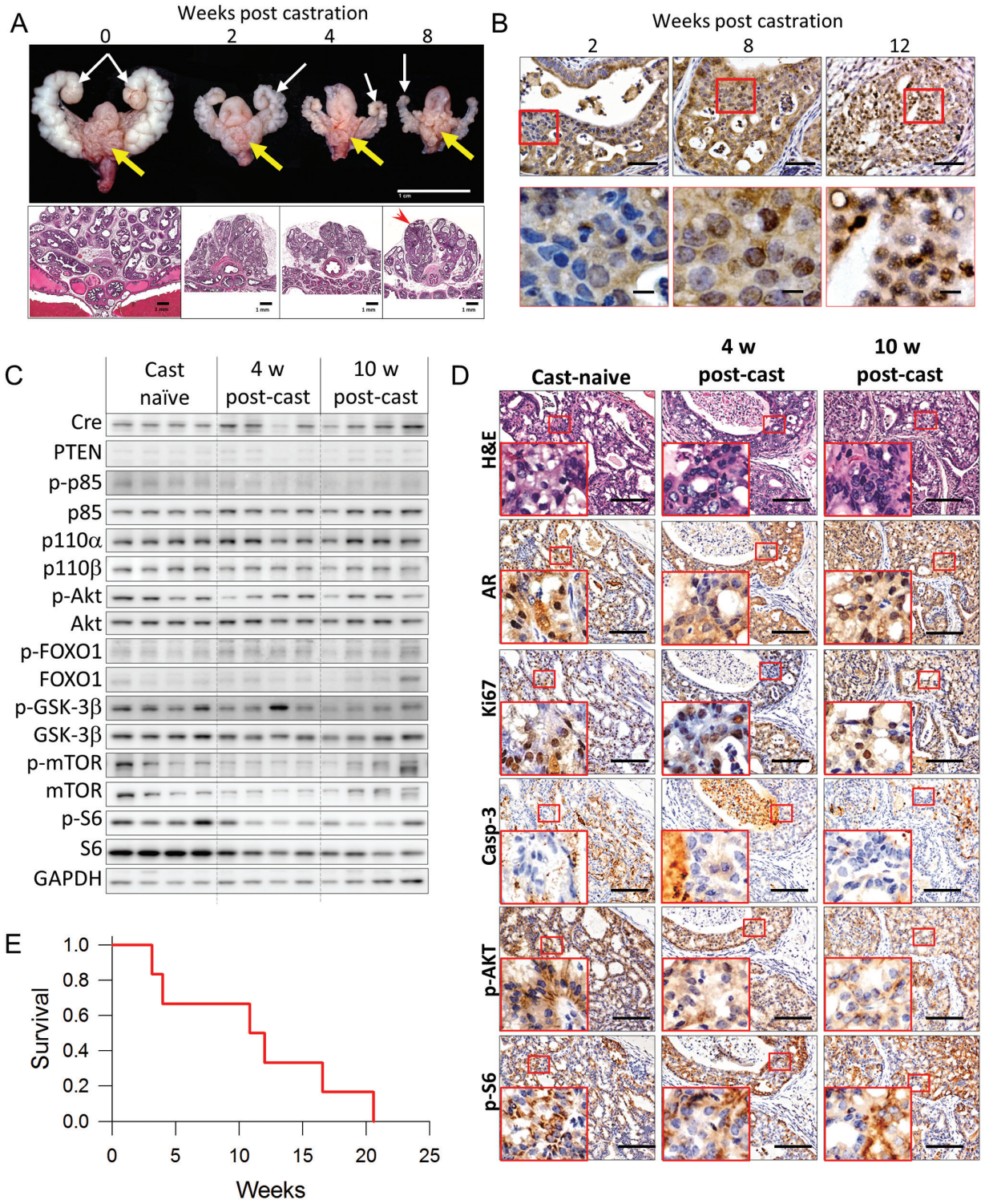

Fig. 2. Androgen deprivation leads to the transformation of CRPC in *PTEN*-deficient tumors. (**A**) Representative images of 20-week-old homozygous *PTEN*-mutant mouse GUTs and their corresponding H&E stained tissue sections demonstrate the effects of androgen deprivation by surgical castration. Both tumor-bearing prostates (yellow arrows) and accessory sex organs (white arrow) demonstrate marked atrophy in response to surgical castration. Note that despite the continued shrinking of the accessory sex organs at 8 weeks post-castration, a notable proportion of glands demonstrate resistance to the effects of androgen deprivation (red arrowhead). Scale bars represent 1.0 cm for gross images and 1.0 mm for low magnification H&E sections. (**B**) Immunohistochemical expression and localization of AR in prostate tumors after surgical castration as indicated. Scale bars represent 100 µm for low magnification and 50 µm for high magnification. (**C**) Expression of Cre, PTEN, PI3K subunits, AKT, AKT substrates and glyceraldehyde 3-phosphate dehydrogenase (GAPDH) by western blotting in prostate tumor lysates collected from mice with androgen dependent tumors without castration (Cast-naive), 4 weeks after castration (Surg. Cast) and mice that developed castration resistant prostate cancer 10 weeks post castration (CRPC). Day of castration was adjusted so all mice were killed at 20 weeks of age. GAPDH was used as a loading control. Original blots are included in Supplementary Figure 7, available at *Carcinogenesis* Online. (**D**) Representative images comparing histology (H&E) and AR, Ki67, cleaved caspase-3, p-AKT and p-S6 IHC expression during the progression to CRPC. Inserts correspond to areas bounded by the red square. Scale bar represents 100 µm. (**E**) Kaplan–Meier curve showing overall survival fraction for homozygous *PTEN*-mutant mice with advanced prostate cancer rates after ADT by surgical castration ($n = 6$).

A decrease in phosphorylated-p85 and p110a and p110b PI3K subunits ware also noted after castration. Consequently, activation of AKT and mammalian target of rapamycin (mTOR) were also decrease. Interestingly levels of p-FOXO1 and p-S6 were not affected by castration (Figure 2C and D). Notably p-GSK3β decreased only in CRPC. To investigate the effects of decreased AKT activity, we next examined the effects of androgen withdrawal on tumor cell proliferation and apoptosis. Tumor proliferation rates in androgen-sensitive tumors were significantly reduced compared with castration-naïve tumor cells, however, proliferation rates were moderately, but significantly recovered in CRPC. The apoptotic index in CRPC was higher than castration-naïve tumors, but lower than that of androgen-sensitive tumors (Figure 2D and Supplementary Figure 3B and C, available at *Carcinogenesis* Online).

Thus far, characterization of androgen withdrawal has been performed in relatively young mice, ~20 weeks of age, which are more representative of early disease. To simulate the effects of androgen deprivation therapy (ADT) on advanced mouse prostate cancer, we evaluated the effects of surgical castration in homozygous *PTEN*-mutant mice with moderate tumor burden. The aim was to determine if hormonal withdrawal would provide a therapeutic effect by deterring disease progression and/or increasing survival. Six mice (median age at castration, 81.8 weeks, range 72.4–87.8 weeks) were included in the cohort. Mean overall survival was 11.2 weeks (95% CI 5.7–16.7, Figure 2E). Median cumulative survival was 89.3 weeks (95% CI 73.7–104.9) compared with 87.3 weeks (95% CI 77.9–96.7, $n = 12$) in castration-naive control mice ($P = 0.621$, Supplementary Figure 3D, available at *Carcinogenesis* Online). No difference in tumor burden was observed between the castrated cohort and castration-naive (Supplementary Figure 3E, available at *Carcinogenesis* Online). In essence, ADT by surgical castration did not improve the prognosis for mice with advanced *PSA-Cre*-driven *PTEN*-deficient prostate cancer demonstrating strikingly similar characteristics of the human disease. These findings suggest that other signaling pathway may be responsible for tumor survival after ADT.

Tumor progression and intratumoral heterogeneity in PTEN-deficient prostate adenocarcinomas

Human prostate cancer is a complex heterogeneous disease characterized by the activation of multiple pathways contributing to its progression. Therefore, to further investigate the clinical suitability of this model, we characterized the expression levels of key pathways associated with cancer progression in humans (21). As expected, inactivation of *PTEN* leads to increased PI3K signal activation over time as indicated by the increased levels of p-AKT and it substrates (Figure 3A and B). In the early tumor stages, signal transduction is dominated primarily by the AR signaling (Figure 3A and B). However, during the progression stages, levels of JAK/STAT3 and mitogen-activated protein kinase (MAPK) signaling increase. This result suggests that as tumors progress heterogeneous cell populations develop. Immunohistochemical analysis from advanced cancer clearly illustrates intratumoral heterogeneity at this stage of the disease (Figure 3C). These finding provides support for plasticity of tumor cells to develop heterogeneous cell populations during the natural progression of *PTEN*-deficient prostate cancer.

The evolution to CRPC promotes intratumoral heterogeneity in PTEN-deficient prostate adenocarcinomas

Heterogeneity in tumors is probably to be one of the major factors contributing to limited treatment efficacy in single-agent therapeutic strategies (22). To determine if ADT promotes phenotypic plasticity leading to increased heterogeneity and to gain insights into the molecular evolution of CRPC in the current mouse model, we used PI3K/AKT/mTOR, MAPK and JAK/STAT3 pathway activation as biological biomarkers to identify heterogeneous phenotypes in tumors from mice with CRPC. We used 20-week-old mice to compare the effects of ADT because tumors from castration-naive mice are characteristically uniform at this stage of development (Figure 3D and E). On the whole, mice that developed CRPC demonstrated increased expression levels of p-extracellular signal-regulated kinase (p-ERK) and p-STAT3-(pY107 and py727) indicating upregulation of MAPK and JAK/STAT3 signal cascades, respectively. Additionally, there was a higher degree of inter-tumor variation signifying that tumor cells respond differently to ADT and that the transformation to CRPC may also lead to promote intratumoral heterogeneity.

To confirm this notion, we next examined expression patterns of signal pathway activation in cancer cells from matched tissue samples corresponding to those used for the western blot assays by IHC to determine the degree of intratumoral heterogeneity. Indeed, our analyses revealed a high degree of intra-tumor variation that was characterized by distinct morphological and immunohistochemical features within the individual tumors. Overall tumor IHC expression patterns closely resembled the western blot data. We illustrate by comparing expression between AR, p-AKT p-S6, p-ERK and p-STAT3 in castration-naive and CRPC (Figure 3F and Supplementary Figure 4, available at *Carcinogenesis* Online). Clearly, p-AKT and S6 were strongly and uniformly expressed in all cancerous glands from castration-naive mice. Conversely, a high degree of inter- and intra-glandular variability of p-AKT and p-S6 expression patterns was observed in CRPC tissues. Furthermore, there were differences in the expression patterns of p-ERK and p-STAT3 in castration-naive and CRPC cells. In castration-naive tumors, p-ERK was focally expressed in luminal cells and general expression patterns did not vary much between mice. However, the overall of p-ERK expression increased in CPPC and positive staining was present in both basal and luminal epithelial cells. Additionally, a high degree of inter- and intra-tumor variability was observed. Expression of p-STAT3-(Tyr705) was predominantly found in the basal layer of castration-naive prostate cancer but was variably expressed in CRPC. Largely, the level of heterogeneity of these signal transduction pathways was similar between mice with advanced castration-naive prostate cancer (>70 weeks of age) and tumors from mice with CRPC at 20 weeks. These findings demonstrate that the PI3K/AKT/mTOR pathway is preferential activated in indolent castration-naive cancers and that the transformation to CRPC drives plasticity in cancer cells that is characterized by unique molecular signatures.

CRPC is resistant to PI3K/AKT/mTOR signaling inhibition

We hypothesize that heterogeneity in CRPC makes the tumors more resistant to targeted therapy compared with castration-naive cancers. To test our hypothesis, we decided to compare the effects of targeting the PI3K/AKT/mTOR signaling axis in castration-naive and CRPCs. We chose mTOR as a target since our observations point to the dependence on PI3K/AKT/mTOR signaling by castration-naive tumors (Figure 3A). In addition, rapalogs, including everolimus, have been widely studied and have demonstrated relative efficacy in other preclinical models of prostate cancer and were the first inhibitors used in clinical trials (23). Yet, these have experienced limited effects in the clinical setting (24–26). To model this scenario, we used everolimus to probe the effects of mTOR inhibition in castration-naive and CRPCs driven by the loss of *PTEN* (Supplementary Figure 5A, available at *Carcinogenesis* Online). Tumor burden was significantly reduced in castration-naive but not castration-resistant tumors after treatment with everolimus (Figure 4A and B). Tumors in castration-naive mice showed obvious histological changes, but few changes were noted in castration-resistant tumors (Figure 4A). Treatment with everolimus effectively inhibited the PI3K/AKT/mTOR signaling axis in both castration-naive and castration-resistant tumors, as evident by the inhibition of p-S6 (Figure 4C and E, and Supplementary Figure 5B, available at *Carcinogenesis* Online). However, levels of p-AKT, p-FOXO1 and p-4E-BP1 increased after treatment indicating negative feedback. Everolimus-treated mice experienced significant reductions tumor proliferation rates in both treatment groups and induced apoptosis in castration-naive cancers but not CRPC (Figure 4C and D).

We next examined the activation of compensatory signaling pathways in response to treatment with everolimus. Inhibition of PI3K/AKT/mTOR signaling resulted in upregulation of MAPK activation

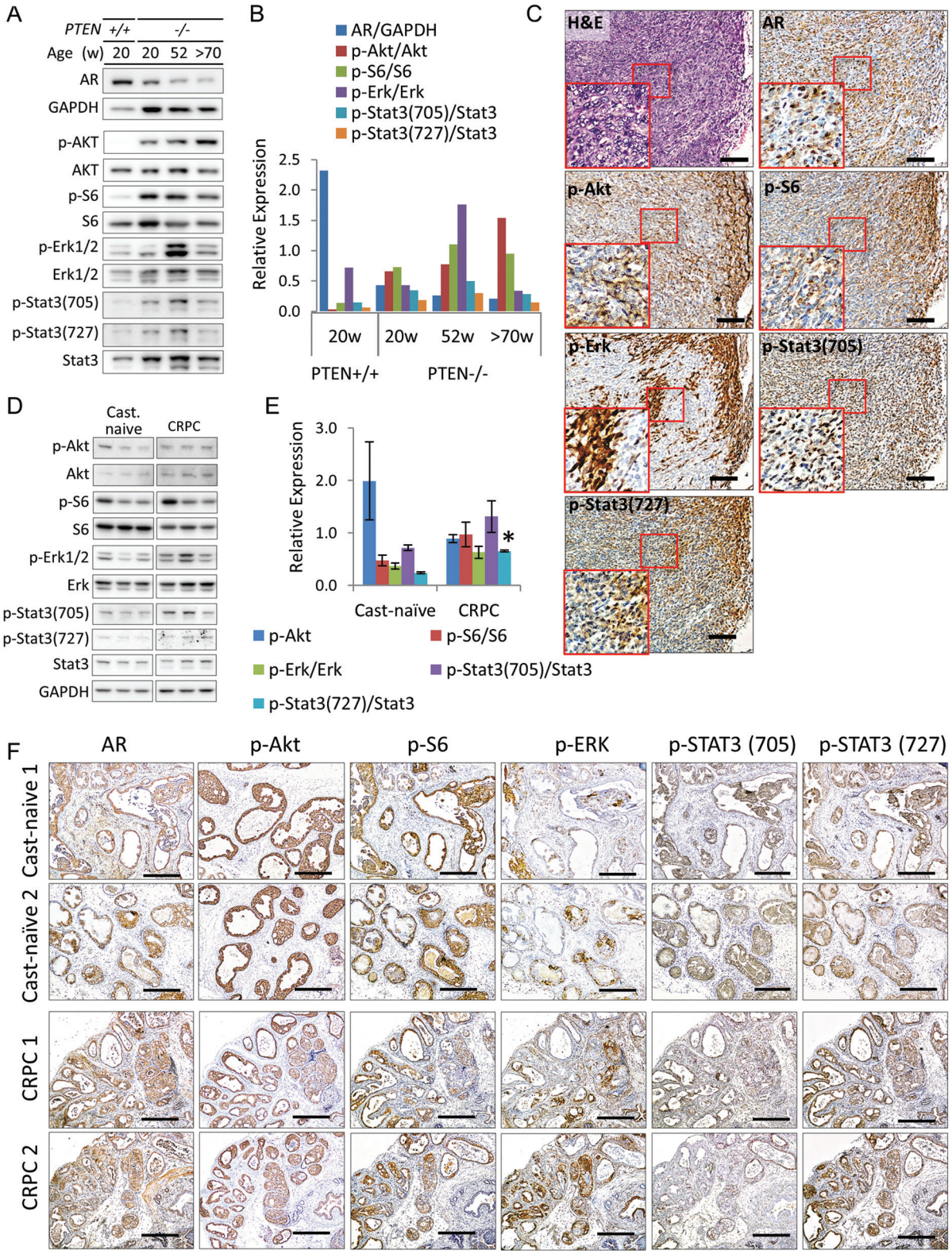

Fig. 3. Intratumoral heterogeneity in *PTEN*-deficient mouse prostate cancer. (**A**) Expression of AR, phosphorylated (p-AKT, p-S6, p-ERK1/2, p-STAT3-(pY705) and p-STAT3-(pY727)) and total protein (AKT, S6, ERK1/2 and STAT3) in pooled prostate tumor lysates (three mice per group) collected from castration-naive wild-type and *PTEN*-deficient mice at indicated ages. Original blots are included in Supplementary Figure 8, available at *Carcinogenesis* Online. (**B**) Densitometric analysis of (A). (**C**) Representative images showing the histological and IHC staining patterns of key downstream pathways molecules in advanced castration-naive mouse prostate cancer at 72 weeks of age. Inserts correspond to boxed region, scale bars represent 100 µm. (**D**) Expression of phosphorylated (p-AKT, p-S6, p-ERK1/2, p-STAT3-(pY705) and p-STAT3-(pY727)) and total protein (AKT, S6, ERK1/2 and STAT3) in individual 20-week-old mice with castration-naive and CRPC. glyceraldehyde 3-phosphate dehydrogenase (GAPDH) was used as a loading control. Original blots are included in Supplementary Figure 9, available at *Carcinogenesis* Online. (**E**) Densitometric analysis of (D, *$P \leq 0.05$ versus castration-naive cancer). (**F**) Representative H&E staining and IHC expression analysis of AR, p-AKT, p-S6, p-ERK1/2, p-STAT3-(pY705) and p-STAT3-(pY727) in prostate tumors from (D), scale bars represent 250 µm. Protein levels were normalized to GAPDH or total protein for all densitometric analyses.

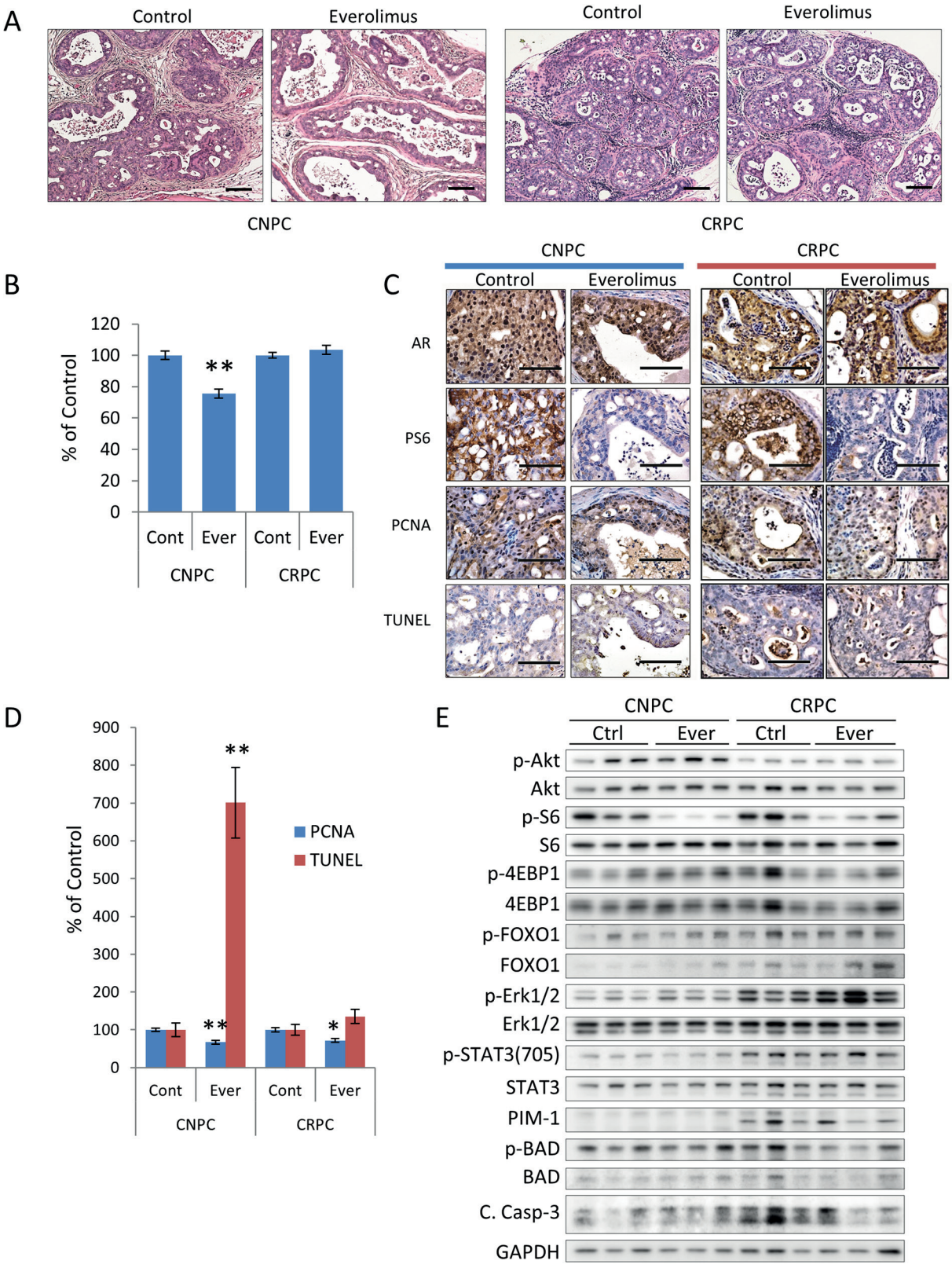

Fig. 4. Therapeutic effect of PI3K inhibition in *PTEN*-deficient prostate cancers. *PTEN*-deficient mice with established castration-naive or CRPC were treated with everolimus (10 mg/kg 3×/wk for 4 weeks, $n = 8$ mice/group) (**A**) Representative H&E stained cross-sections of mouse GUT. Scale bars represent 50 µm. (**B**) Tumor burden was assessed by the GUT weight normalized to control mice and expressed as the mean ± SE (*$P < 0.001$ versus control). (**C**) Representative photomicrographs of tumor sections stained for AR, p-S6, PCNA and terminal deoxynucleotidyl transferase-mediated dUTP nick end labeling (TUNEL) assay. Scale bars equal 50 µm. (**D**) Plots of the relative differences in the cellular proliferation rates (measured by the mean ± SE percentage of PCNA-positive cells) and the apoptotic index (measured by the mean ± SE percentage of cells positive for the TUNEL assay, *$P < 0.05$, **$P < 0.001$ versus control). (**E**) Expression of AKT, AKT substrates, and phosphorylated and total ERK1/2, and STAT3- in prostate tumor lysate samples as indicated. Original blots are included in Supplementary Figure 10, available at *Carcinogenesis* Online.

in both castration-naive and castration-resistant tumors (Figure 4E, Supplementary Figure 5B, available at *Carcinogenesis* Online). The response of MAPK activation between mice with castration-naive tumors was fairly uniform. Interestingly, responses to MAPK activation varied noticeably in mice with CRPC. This result suggests that levels of MAPK activation in CRPC tumors are not only a result of compensatory signaling due to PI3K inhibition, but also reflect differences in the populations of cells that are dependent on MAPK activation for growth and survival. STAT3 signaling showed only a slight increase in response to treatment with everolimus. Since PIM-1 kinase has been associated with therapeutic resistance to PI3K inhibitors (27), we investigated the expression levels of PIM-1 kinase and inactivation of the pro-apoptotic protein, BAD. Mice with CRPC demonstrated increased levels of PIM-1, however, BAD phosphorylation decreased after treatment with everolimus suggesting that PIM kinase signaling may be not be involved in survival.

Dual inhibition of PI3K/AKT/mTOR and MAPK signal inhibition cooperate to restore therapeutic efficacy in CRPC

To determine if dual blockade of mTOR and MAPK inhibition improved treatment efficacy in CRPC, we treated mice with everolimus in combination with the MEK1/2 inhibitor U0126 using the previous treatment schedule. We used U0126 since it has been shown to inhibit MAPK activity and suppress tumor cells *in vivo* (28). Interestingly, treating castration-naive cancers with mTOR or MAPK inhibition was effective as monotherapy, but not improved when used in combination. In contrast, monotherapy with either everolimus or U0126 alone led to therapeutic escape in CRPC, which was however was overcome by combination therapy (Figure 5A and B). A comparison of treatment responses according to treatment demonstrates differences between sensitivity and the differential responses to monotherapy and combination therapy in castration-naive and CRPC (Figure 5C). Histopathological analysis of CRPC-treated mice demonstrated no changes in tumor proliferation rates, but did reveal increased apoptotic rates in mice receiving combination therapy (Figure 5D and E).

Finally, we confirmed target specificity and pathway activation responses to combination therapy in CRPC. Everolimus effectively inhibited p-S6 but was not augmented by U0126., however, p-ERK was for the most part decreased however, some mice demonstrated resistance to U0126 (Figure 6A and B and Supplementary Figure 5A, and Supplementary Figure 12, available at *Carcinogenesis* Online) However, mice receiving the combination therapy experienced a significant inhibition of ERK phosphorylation. Overall levels of p-4E-BP1 increased significantly after combination therapy (Figure 6A and Supplementary Figure 6A, available at *Carcinogenesis* Online). We examined STAT3, PIM-1 and BAD levels in response to combination therapy of mTOR and MAPK inhibition therapy. Levels of p-STAT3 did not change much after drug administration and PIM levels were elevated in after treatment with U0126 alone or in combination (Supplementary Figures 6B and 12, available at *Carcinogenesis* Online). However, the levels of BAD phosphorylation decreased after combination treatment. Together, these sets of experiments confer resistance to single agent inhibition in CRPC and demonstrate that therapeutic escape can be overcome with a rational therapeutic approach.

Discussion

Herein, we used a conditional *PTEN*-deficient mouse model of prostate cancer to show that intratumoral heterogeneity is an important manifestation in the evolution to CRPC and is a significant contributor to therapeutic escape. We focused on *PTEN* inactivation due to its prevalence and biological significance in human prostate cancer, and its role as one of the earliest tumor initiating events in prostate tumorigenesis (29). Inactivation of *PTEN* is commonly observed in human prostate cancer (11) and is also believed to contribute to AR resistance (4,5). In our animal model, inactivation of *PTEN*, driven by the 6-kb fragment of the human *PSA* promoter, targets the luminal cells of the adult prostate (17). We selected a *PSA* promoter over probasin-based promoters since these target both basal and luminal cells of prostate glands and the seminal vesicles in developing and mature animals (30). Ma *et al.* (31) previously reported a *PSA-Cre;PTEN*^{loxP} model of prostate cancer, however, their model was generated on a mixed 129Ola/FVB genetic background. Genetic background is known to affect the phenotypic expression of a gene mutation, thus a mixed background introduces an unwanted variable for the phenotypic and molecular characterization of tumors (32,33). We based our model on a pure C57Bl6/J background strain, hence, it incorporates features of adult prostate tumorigenesis while eliminating the complexity of strain-dependent differences in gene expression.

Tumor latency in our homozygous *PTEN*-mutant mice is within the spectrum reported in other tumor models based on *PTEN* inactivation (14). Penetrance of *PSA-Cre* was observed in the prostate shortly after puberty, which is in agreement with previous reports using the same promoter (15,17). Even though all mice develop tumors progression is slow and survival is long. Therefore, our model supports the notion that inactivation of *PTEN* is involved primarily in the initiation of prostate cancer but less so in progression conferring that other genetic alteration(s) are required to promote more aggressive tumors such as the inactivation of *P53* (*Trp53*) (34) and *SMAD4* (35) or the activation of *K-Ra* (36), which have been shown to cooperate with *PTEN* to produce more aggressive phenotypes.

Similar to other mouse models of prostate cancer, tumors from our *PTEN*-deficient mouse model experience an initial response to ADT that is followed by the eventual development of CRPC (4,5,37,38,39). Furthermore, we show that a high degree of heterogeneity exists with regards to the re-expression of nuclear AR in actively proliferating cancer cells from CRPC tumors. This feature is also noted in clinical samples of advanced prostate cancer (40). Most notably, we show that ADT did not deter disease progression nor did it improve survival supporting support the notion that targeting the AR signaling axis alone is not enough to deter tumor survival and alternative compensatory signaling pathways play key roles the growth and survival of tumors. Notably, levels p-AKT and the PI3K subunits decreased after castration. Still, levels of some of its substrates remained active and more importantly the tumors continued to proliferate. We suspect that this effect may be attributable to a feedback regulation loop of PI3K/Akt via the adaptor protein, IRS-1 and PI3K p85 regulatory subunit. Studies have shown that persistent activation of the mTOR/S6-kinase pathway can lead to feedback inhibition of PI3K signaling through upstream activators such the adaptor protein, insulin receptor substrate 1 (IRS-1) (41). Another possibility is that transcriptional activation of AR could have negatively regulated AKT by stimulating FKBP5 and PHLPP (4). Castration-naive tumors grew slowly and developed uniformly during the early stages, but showed a higher degree of phenotypic and molecular heterogeneity with age. We also showed that activation of signal pathways associated with CRPC, such as MAPK and JAK/STAT3, were similarly upregulated in mice with early early-stage tumors that developed CRPC as a result of ADT. Moreover, our drug intervention studies demonstrated that survival in these tumors as a whole did not appear to be dominated by any one particular signal transduction pathway as compared with early castration-naive tumors which are generally dominated by PI3K/AKT/mTOR signaling.

Given the role of *PTEN* in prostate cancer, a number of treatment strategies aimed at inhibiting PI3K signaling are currently being developed and tested. The PI3K/AKT/mTOR signaling axis provides a direct link for the development of prostate cancer. For example, it is now well-established that inactivation of *PTEN* in prostate leads to the development of cancer, however, deletion of mTOR in prostate cells inhibited tumor development in mouse *PTEN*-deficient prostates (42). The increase of AKT/S6 activation, due to the inactivation of *PTEN*, suggested that tumors from these mice would be highly dependent on PI3K signaling for growth and survival. For this reason, we elected to focus on the PI3K/AKT/mTOR signaling axis to compare treatment responses. Castration-naive tumors responded well to PI3K/AKT/mTOR pathway inhibition. These findings were consistent with other published reports (43–45). However, mice harboring CRPC failed to

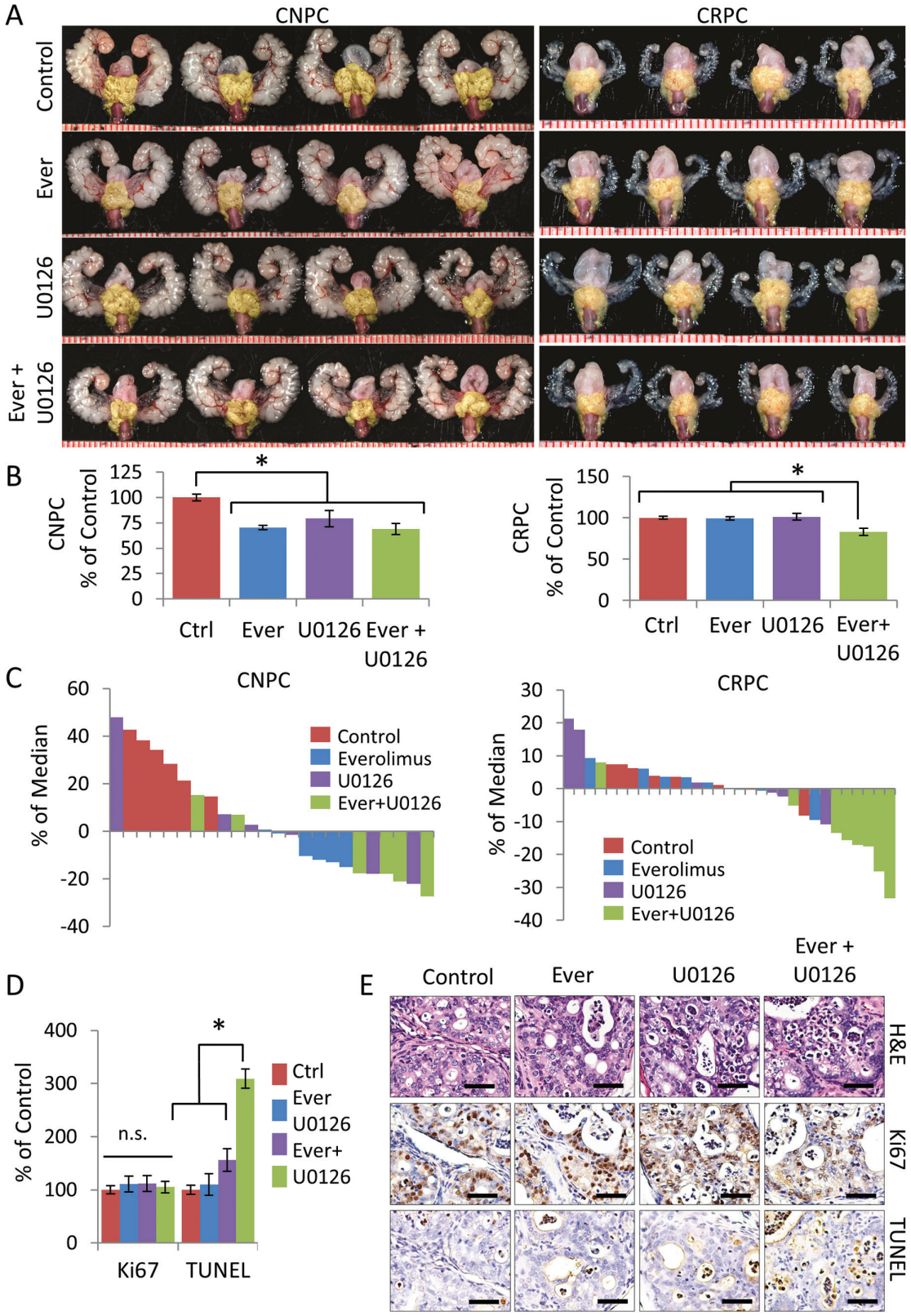

Fig. 5. Dual inhibition of mTOR and MAPK reverses therapeutic escape of CRPC. 20-week-old *PTEN*-deficient mice with castration-naive ($n = 6$ mice/group) or CRPC ($n = 8$ mice/group) were treated with everolimus or U0126 for 4 weeks as described in Materials and Methods. (**A**) Representative GUTs from mice after indicated treatment. Prostate tumors are highlighted in yellow. Scale is represented in mm. (**B**) Plots of tumor burden was assessed by tumor area normalized to control mice and expressed as the mean ± SE, $^*P \leq 0.001$ versus control. (**C**) Waterfall plot of relative tumor burden with treatment correlates. (**D**) Plots of the relative cellular proliferation rates (measured by the mean ± SE percentage of Ki67-positive cells) and the apoptotic index (measured by the mean ± SE percentage of cells positive for the terminal deoxynucleotidyl transferase-mediated dUTP nick end labeling (TUNEL) assay, $^*P \leq 0.01$ versus control) or CRPC mice treated as indicated. (**E**) Representative sections from control and treated CRPC tumors stained with H&E, KI67 and TUNEL. Scale bars represent 50 μm.

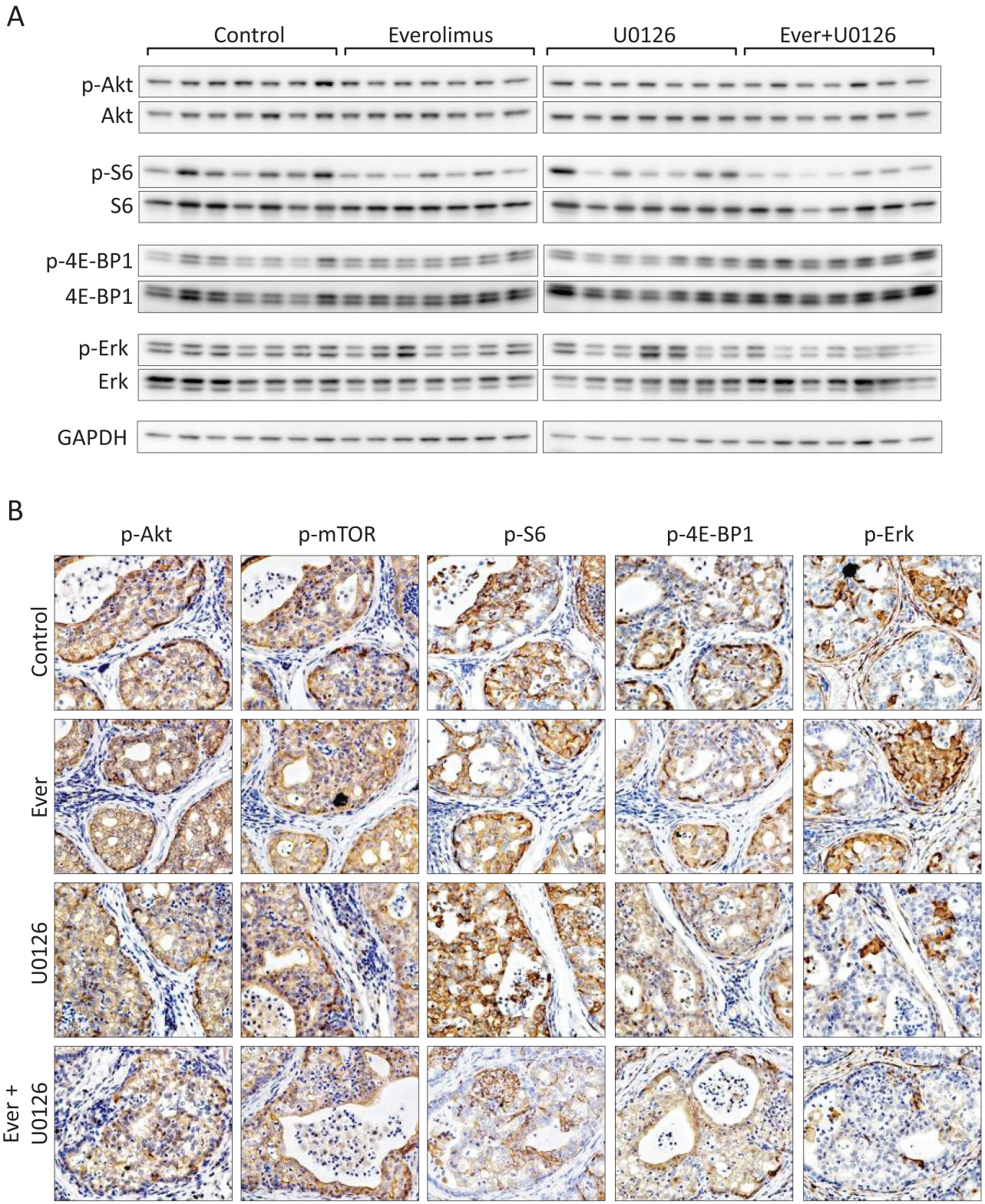

Fig. 6. Molecular responses to combined inhibition of mTOR and MAPK signaling in CRPC. (**A**) Expression of AKT, AKT substrates, and phosphorylated and total ERK1/2 in prostate tumor lysate samples from CRPC after the indicated treatments. Original blots are included in Supplementary Figure 11, available at *Carcinogenesis* Online. (**B**) Representative photomicrographs of p-AKT, p-mTOR, p-S6, p-4E-BP1 and p-ERK expression in CRPC mice after mono- and combination therapy with everolimus an U0126.

achieve a treatment response. The lack of efficacy from mTOR inhibitors can occur by various feedback control circuits (46). However, responses after treatment with everolimus differed between CRPC and castration-naive cancers. For example, differences between MAPK pathway activation in CRPC and castration-naive cancer in response to mTOR inhibition suggest that pathway activation is probably a reflection of phenotypic heterogeneity in CRPC. Thus far, the precise mechanisms that drive plasticity in castration-resistant cancer

cells are still under investigation, but evidence points to a paracrine-to-autocrine shift in the regulation of homeostasis by cancer cells (47) in addition to changes in stromal–epithelial interactions (48), and inflammation (49). In summary, our experimental model shows that ADT leads to CRPC which in turn contributes to the clonal evolution and expansion of treatment-insensitive subclones that are less dependent on PI3K/AKT/mTOR signaling axis for survival and reinforces the notion that multiple targets must be challenged in order to achieve any significant treatment responses.

In conclusion, our findings demonstrate that the transformation to CRPC in *PTEN*-deficient tumors leads to phenotypic plasticity, an adaptive mechanism that results in the development of tumors with an acquired resistance. Thus, incorporating intratumoral heterogeneity in a dynamic tumor model as part of preclinical efficacy determination could in turn provide better a better understanding of drug responses and would allow for improved prediction of novel treatment strategies.

Supplementary material

Supplementary Tables 1 and 2 and Supplementary Figures 1–12 can be found at http://carcin.oxfordjournals.org/

Funding

Grant-in-Aid for Scientific Research from the Japan Society for the Promotion of Science (22591781 to M.A.D.V.).

Acknowledgements

The authors would like to thank Drs Jeffrey Milbrandt and Tak Mak for kindly sharing their animals. The authors would also like to thank Ms Yurie Kura, Ms Naomi Ando, Mrs Emiko Fukushima, Mr Hideki Nakagaki and Mrs Mieko Nishio for their technical assistance and Dr Nobuyuki Mizoguchi and members of Kinki University Animal Core Facility for their excellent veterinary support.

Conflict of Interest Statement: None declared.

References

1. Decker,K.F. *et al.* (2012) Persistent androgen receptor-mediated transcription in castration-resistant prostate cancer under androgen-deprived conditions. *Nucleic Acids Res*., **40**, 10765–10779.
2. Ha,S. *et al.* (2011) Androgen receptor levels are upregulated by Akt in prostate cancer. *Endocr. Relat. Cancer*, **18**, 245–255.
3. Ryan,C.J. *et al.* (2011) Androgen receptor rediscovered: the new biology and targeting the androgen receptor therapeutically. *J. Clin. Oncol*., **29**, 3651–3658.
4. Mulholland,D.J. *et al.* (2011) Cell autonomous role of PTEN in regulating castration-resistant prostate cancer growth. *Cancer Cell*, **19**, 792–804.
5. Carver,B.S. *et al.* (2011) Reciprocal feedback regulation of PI3K and androgen receptor signaling in PTEN-deficient prostate cancer. *Cancer Cell*, **19**, 575–586.
6. Reynolds,M.A. (2008) Molecular alterations in prostate cancer. *Cancer Lett*., **271**, 13–24.
7. Kola,I. *et al.* (2004) Can the pharmaceutical industry reduce attrition rates? *Nat. Rev. Drug Discov*., **3**, 711–715.
8. Kitano,H. (2004) Cancer as a robust system: implications for anticancer therapy. *Nat. Rev. Cancer*, **4**, 227–235.
9. Amit,I. *et al.* (2007) Evolvable signaling networks of receptor tyrosine kinases: relevance of robustness to malignancy and to cancer therapy. *Mol. Syst. Biol*., **3**, 151.
10. Maehama,T. *et al.* (1998) The tumor suppressor, PTEN/MMAC1, dephosphorylates the lipid second messenger, phosphatidylinositol 3,4,5-trisphosphate. *J. Biol. Chem*., **273**, 13375–13378.
11. Yoshimoto,M. *et al.* (2007) FISH analysis of 107 prostate cancers shows that PTEN genomic deletion is associated with poor clinical outcome. *Br. J. Cancer*, **97**, 678–685.
12. McCall,P. *et al.* (2008) Is PTEN loss associated with clinical outcome measures in human prostate cancer? *Br. J. Cancer*, **99**, 1296–1301.
13. Davies,M.A. (2011) Regulation, role, and targeting of Akt in cancer. *J. Clin. Oncol*., **29**, 4715–4717.
14. De Velasco,M.A. *et al.* (2012) Preclinical remodeling of human prostate cancer through the PTEN/AKT pathway. *Adv. Urol*., **2012**, 419348.
15. Abdulkadir,S.A. *et al.* (2002) Loss of Nkx3.1 in adult mice induces prostatic Intraepithelial neoplasia. *Mol. Cell Biol*., **22**, 1495–1503.
16. Suzuki,A. *et al.* (2001) T cell-specific loss of Pten leads to defects in central and peripheral tolerance. *Immunity*, **14**, 523–534.
17. Cleutjens,K.B. *et al.* (1997) A 6-kb promoter fragment mimics in transgenic mice the prostate-specific and androgen-regulated expression of the endogenous prostate-specific antigen gene in humans. *Mol. Endocrinol*., **11**, 1256–1265.
18. Tomioka,A. *et al.* (2008) Delivery of PTEN via a novel gene microcapsule sensitizes prostate cancer cells to irradiation. *Mol. Cancer Ther*., **7**, 1864–1870.
19. Shappell,S.B. *et al.* (2004) Prostate pathology of genetically engineered mice: definitions and classification. The consensus report from the Bar Harbor meeting of the Mouse Models of Human Cancer Consortium Prostate Pathology Committee. *Cancer Res*., **64**, 2270–2305.
20. Ittmann,M. *et al.* (2013) Animal models of human prostate cancer: the consensus report of the New York meeting of the Mouse Models of Human Cancers Consortium Prostate Pathology Committee. *Cancer Res*., **73**, 2718–2736.
21. Lee,J.T. *et al.* (2008) Targeting prostate cancer based on signal transduction and cell cycle pathways. *Cell Cycle*, **7**, 1745–1762.
22. Calderwooed,S.A. (2013) Tumor heterogeneity, clonal evolution, and therapy resistance: an opportunity for multitargeting therapy. *Discov. Med*., **82**, 188–194.
23. Bitting,R.L., *et al.* (2013). Targeting the PI3K/Akt/mTOR pathway in castration-resistant prostate cancer. *Endocr. Relat. Cancer*., **20**, R83–R99.
24. Armstrong,A.J. *et al.* (2010) A pharmacodynamic study of rapamycin in men with intermediate- to high-risk localized prostate cancer. *Clin. Cancer Res*., **16**, 3057–3066.
25 Templeton,A.J. *et al.* (2013) Phase 2 trial of single-agent everolimus in chemotherapy-naive patients with castration-resistant prostate cancer (SAKK 08/08). *Eur. Urol*., **64**, 150–158.
26. Nakabayashi,M. *et al.* (2012) Phase II trial of RAD001 and bicalutamide for castration-resistant prostate cancer. *BJU Int*., **110**, 1729–1735.
27. Schatz,J.H. *et al.* (2011) Targeting cap-dependent translation blocks converging survival signals by AKT and PIM kinases in lymphoma. *J. Exp. Med*., **208**, 1799–1807.
28. Marampon,F. *et al.* (2011) MEK/ERK inhibitor U0126 increases the radiosensitivity of rhabdomyosarcoma cells *in vitro* and *in vivo* by downregulating growth and DNA repair signals. *Mol. Cancer Ther*., **10**, 159–168.
29. Hill,R. *et al.* (2009) PTEN, stem cells, and cancer stem cells. *J. Biol. Chem*., **284**, 11755–11759.
30. Parisotto,M. *et al.* (2013) Genetically engineered mouse models of prostate cancer. *Mol. Oncol*., **7**, 190–205.
31. Ma,X. *et al.* (2005) Targeted biallelic inactivation of Pten in the mouse prostate leads to prostate cancer accompanied by increased epithelial cell proliferation but not by reduced apoptosis. *Cancer Res*., **65**, 5730–5739.
32. Montagutelli,X. (2000) Effect of the genetic background on the phenotype of mouse mutations. *J. Am. Soc. Nephrol*., **16**, S101–S105.
33. Freeman,D. *et al.* (2006) Genetic background controls tumor development in PTEN-deficient mice. *Cancer Res*., **66**, 6492–6496.
34. Chen,Z. *et al.* (2005) Crucial role of p53-dependent cellular senescence in suppression of Pten-deficient tumorigenesis. *Nature*, **436**, 725–730.
35. Ding,Z. *et al.* (2011) SMAD4-dependent barrier constrains prostate cancer growth and metastatic progression. *Nature*, **470**, 269–273.
36. Mulholland,D.J. *et al.* (2012) Pten loss and RAS/MAPK activation cooperate to promote EMT and metastasis initiated from prostate cancer stem/progenitor cells. *Cancer Res*., **72**, 1878–1889.
37. Wang,S. *et al.* (2003) Prostate-specific deletion of the murine Pten tumor suppressor gene leads to metastatic prostate cancer. *Cancer Cell*, **4**, 209–221.
38. Zhang,W. *et al.* (2009) Inhibition of tumor growth progression by antiandrogens and mTOR inhibitor in a Pten-deficient mouse model of prostate cancer. *Cancer Res*., **69**, 7466–7472.
39. Floc'h,N. *et al.* (2012) Dual targeting of the Akt/mTOR signaling pathway inhibits castration-resistant prostate cancer in a genetically engineered mouse model. *Cancer Res*., **72**, 4483–4493.
40. Roudier,M.P. *et al.* (2003) Phenotypic heterogeneity of end-stage prostate carcinoma metastatic to bone. *Hum. Pathol*., **34**, 646–653.
41. Luo,J. *et al.* (2005). The negative regulation of phosphoinositide 3-kinase signaling by p85. *Cell Cycle*, **4**, 1309–1312.
42. Guertin,D.A. *et al.* (2009) mTOR complex 2 is required for the development of prostate cancer induced by Pten loss in mice. *Cancer Cell*, **15**, 148–159.

43. Podsypanina,K. *et al.* (2001) An inhibitor of mTOR reduces neoplasia and normalizes p70/S6 kinase activity in Pten+/- mice. *Proc. Natl Acad. Sci. USA*, **98**, 10320–10325.
44. Majumder,P.K. *et al.* (2004) mTOR inhibition reverses Akt-dependent prostate intraepithelial neoplasia through regulation of apoptotic and HIF-1-dependent pathways. *Nat. Med*., **10**, 594–601.
45. Kinkade,C.W. *et al.* (2008) Targeting AKT/mTOR and ERK MAPK signaling inhibits hormone-refractory prostate cancer in a preclinical mouse model. *J. Clin. Invest*., **118**, 3051–3064.
46. Rodrik-Outmezguine,V.S. *et al.* (2011) mTOR kinase inhibition causes feedback-dependent biphasic regulation of AKT signaling. *Cancer Discov*., **1**, 248–259.
47. Gao,J. *et al.* (2001) Conversion from a paracrine to an autocrine mechanism of androgen-stimulated growth during malignant transformation of prostatic epithelial cells. *Cancer Res*., **61**, 5038–5044.
48. Arnold,J.T. *et al.* (2002) Mechanisms involved in the progression of androgen-independent prostate cancers: it is not only the cancer cell's fault. *Endocr. Relat. Cancer*, **9**, 61–73.
49. Hölzel,M. *et al.* (2013) Plasticity of tumour and immune cells: a source of heterogeneity and a cause for therapy resistance? *Nat. Rev. Cancer*, **13**, 365–376.

Received December 12, 2013; revised May 30, 2014; accepted June 16, 2014